Received: 8 November 2023 | Revised: 26 December 2023 | Accepted: 31 December 2023

DOI: 10.1002/cey2.538

RESEARCH ARTICLE

CARBON ENERGY WILEY

Lignin-derived hard carbon anode with a robust solid electrolyte interphase for boosted sodium storage performance

Jingqiang Zheng[1] | Yulun Wu[1] | Chaohong Guan[2] | Danjun Wang[1] | Yanqing Lai[1] | Jie Li[1] | Fuhua Yang[3] | Simin Li[1] | Zhian Zhang[1]

[1]Hunan Provincial Key Laboratory of Nonferrous Value-Added Metallurgy, National Energy Metal Resources and New Materials Key Laboratory, School of Metallurgy and Environment, Engineering Research Center of the Ministry of Education for Advanced Battery Materials, Central South University, Changsha, China

[2]University of Michigan-Shanghai Jiao Tong University Joint Institute, Shanghai Jiao Tong University, Shanghai, China

[3]Helmholtz Institute Ulm, Ulm, Germany

Correspondence
Fuhua Yang, Helmholtz Institute Ulm, Helmholtzstrasse 11, D-89081 Ulm, Germany.
Email: fuhua.yang@kit.edu

Simin Li and Zhian Zhang, Hunan Provincial Key Laboratory of Nonferrous Value-Added Metallurgy, National Energy Metal Resources and New Materials Key Laboratory, School of Metallurgy and Environment, Engineering Research Center of the Ministry of Education for Advanced Battery Materials, Central South University, 410083 Changsha, China.
Email: simin.li@csu.edu.cn and zhangzhian@csu.edu.cn

Funding information
National Natural Science Foundation of China, Grant/Award Numbers: 52274309, 52204327; Postgraduate Scientific Research Innovation Project of Hunan Province, Grant/Award Number: CX20220183

Abstract

Hard carbon is regarded as a promising anode candidate for sodium-ion batteries due to its low cost, relatively low working voltage, and satisfactory specific capacity. However, it still remains a challenge to obtain a high-performance hard carbon anode from cost-effective carbon sources. In addition, the solid electrolyte interphase (SEI) is subjected to continuous rupture during battery cycling, leading to fast capacity decay. Herein, a lignin-based hard carbon with robust SEI is developed to address these issues, effectively killing two birds with one stone. An innovative gas-phase removal-assisted aqueous washing strategy is developed to remove excessive sodium in the precursor to upcycle industrial lignin into high-value hard carbon, which demonstrated an ultrahigh sodium storage capacity of 359 mAh g^{-1}. It is found that the residual sodium components from lignin on hard carbon act as active sites that controllably regulate the composition and morphology of SEI and guide homogeneous SEI growth by a near-shore aggregation mechanism to form thin, dense, and organic-rich SEI. Benefiting from these merits, the as-developed SEI shows fast Na^+ transfer at the interphases and enhanced structural stability, thus preventing SEI rupture and reformation, and ultimately leading to a comprehensive improvement in sodium storage performance.

KEYWORDS
hard carbon, lignin, sodium components, sodium-ion storage, solid electrolyte interphase

1 | INTRODUCTION

The scarcity of lithium resources restricts further application of state-of-the-art lithium-ion batteries (LIBs) in large-scale energy storage systems, for which the top priority is no longer energy density but production cost.[1,2] Sodium-ion batteries (SIBs), which have analogous intercalation chemistry/electrochemistry as LIBs, are considered as promising alternatives to LIBs due to the abundance of sodium resources available.[3–5] The major issue impeding the commercialization of SIBs is the absence of appropriate anode materials. Thermodynamically, the commonly used graphite anodes in LIBs are not suitable in SIBs.[6–8] In 2000, Stevens et al.[9] first reported that hard carbon obtained from glucose pyrolysis delivered reasonable reversible capacity in SIBs, which brought about a turnaround in the development of anode materials for SIBs. Since then, considerable efforts have been devoted toward the synthesis and optimization of hard carbon.[10–14] Notably, the development of high-performance hard carbon with relatively low production costs is crucial for SIBs. Specifically, finding affordable carbon precursors is critical for the realization of low-cost hard carbon, while achievement of excellent electrochemical performance demands high sodium storage capacity and robust interphases to ensure long-term cycle stability.

Biomass has gained attention as a significant feedstock category for the synthesis of hard carbon due to its economic viability and sustainability. However, the heterogeneity of feedstocks presents challenges to its large-scale production. Lignin, which is extracted from biomass, is the second most abundant organic material globally and is anticipated to offer a plethora of valuable hard carbon products.[15] Moreover, alkaline liquor (also known as black liquor), a byproduct derived from processes aimed at cellulose recovery from biomass, serves as an abundant source of industrial lignin. Unfortunately, the frequent utilization of sodium-containing chemicals during the alkaline pulping process for lignin separation from biomass leads to a high sodium content in the extracted industrial lignin (Figure 1A), thereby significantly impeding its conversion into high-value-added carbon products.[16] In fact, lignin-derived hard carbon shows unsatisfactory electrochemical performance, so it is necessary to blend lignin with other precursors such as pitch and polyacrylonitrile to improve the as-prepared hard carbon performance.[17,18] Therefore, the preparation of hard carbon with excellent sodium storage performance using industrial lignin remains a challenge. Considering previous studies reporting the use of residual sodium components on the cathode surface to establish a robust interphase,[19] there is great anticipation for the potential applicability of this concept in the negative electrode.

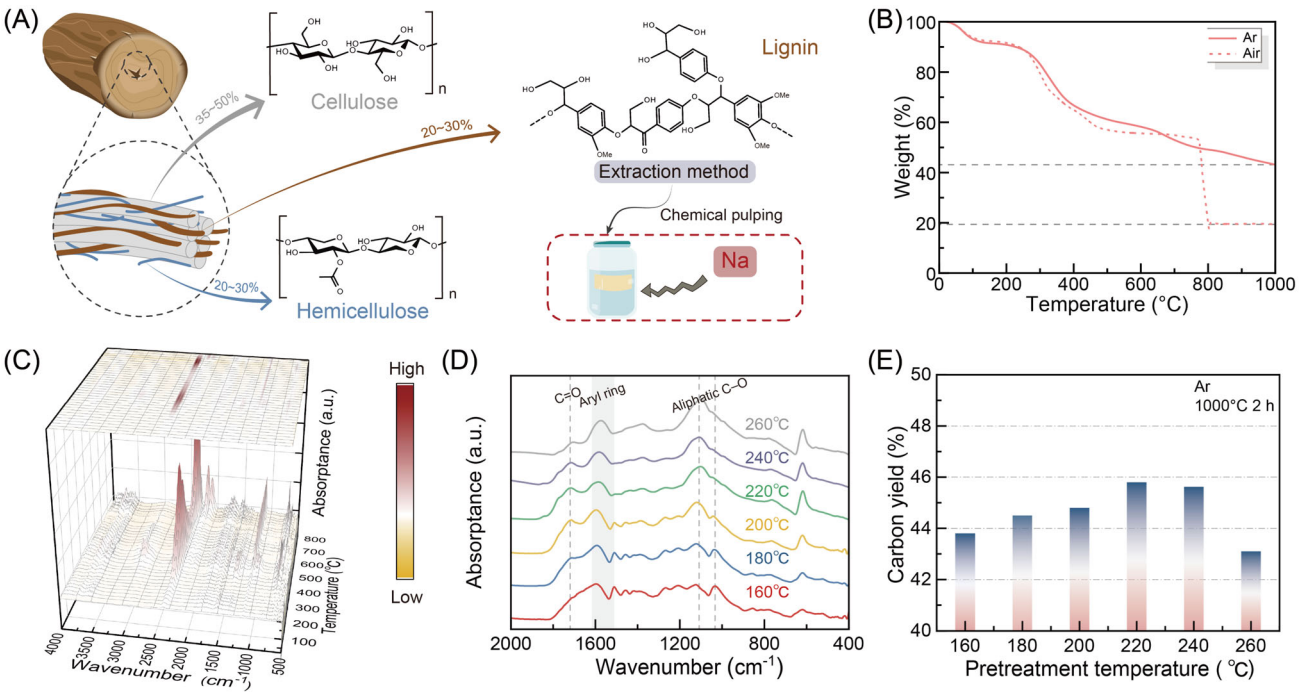

FIGURE 1 (A) Composition and macrostructures of the lignocellulose structure. (B) Weight loss curves for lignin. (C) TGA-FTIR data of lignin. (D) FTIR spectra of lignin pretreated at different temperatures. (E) Carbon yield of lignin pretreated at different temperatures.

In this study, we have successfully developed a hard carbon anode using industrial lignin. The as-developed hard carbon shows excellent electrochemical performance in SIBs in terms of reversible capacity and cycling life. Especially, a gas-phase removal-assisted aqueous washing strategy was proposed to remove sodium components inside the precursor to achieve high sodium storage capacity. Furthermore, it is found that residual sodium components on the as-synthesized hard carbon help to form robust solid electrolyte interphase (SEI) layers, which is beneficial for improving the anode performance. The comprehensive analysis of physical and chemical properties indicates that organic-rich SEI layers are uniformly and densely distributed on the surface of hard carbon. Theoretical calculations elucidate the mechanism underlying the formation of robust SEI, namely, the uniform nucleation deposition of SEI utilizing residual sodium components on the hard carbon surface via a near-shore aggregation mechanism. Hence, the utilization of tailored hard carbon materials, coupled with robust interphases, enables superior electrochemical performance of hard carbon anodes for SIBs. Specifically, a remarkable reversible capacity (359 mAh g^{-1}) and 400 stable cycles are obtained.

2 | RESULTS AND DISCUSSION

2.1 | Synthesis of lignin-derived hard carbon

In the global pulping and paper industry, lignin is produced as a byproduct of the pulping process at about 50 million tons annually.[20] Only a tiny percentage of this lignin is used for value-added products, and the remainder is commonly burned for electricity generation. To highlight the economy and universality of this study, the lignin used in the study was derived from alkali lignin from the pulp industry. Carbon yield is a key indicator for the preparation of hard carbon.[21] Thermogravimetric analysis (TGA) was first performed to determine the carbon yield of lignin pyrolysis (Figure 1B), and it was found that the sample can achieve an approximately 40% carbon yield under an argon atmosphere at 1000°C. However, lignin remains as ~20 wt% residual mass after being ashed up to 1000°C, which can be attributed to the oxidation products of the sodium components in lignin.[22] To determine the reasons for the low carbon yield (organic elemental analysis showed that lignin contained close to 51 wt% of carbon atoms), we used TGA coupled with online gas-phase Fourier transform infrared spectroscopy (FTIR; Figures 1C, S1 and Table S1) and gas chromatography–mass spectrometry (Figure S2) to monitor the gas compositions during lignin thermal evolution. It was found that the sodium components of lignin can affect hard carbon yield by facilitating the release of small molecules and accelerating carbon decomposition (detailed analysis in Text S1).

To achieve higher carbon yields, we implemented a preoxidation strategy to enhance the cross-linking of lignin molecules, thereby inhibiting the release of small molecules during pyrolysis. The functional groups of lignin were monitored by FTIR during air preoxidation at different temperatures (Figure 1D), and the results indicate that the degree of lignin cross-linking increases as the temperature increases.[23] Subsequently, the carbon yield of preoxidation lignin was assessed at different temperatures (Figure 1E). The carbon yield showed an initial increase at lower temperatures with an increase in the pretreatment temperature, reaching a maximum value at 220°C, followed by a subsequent decrease at higher temperatures. This phenomenon can be attributed to the fact that preoxidation enhances the cross-linking between lignin molecules, thereby impeding rapid lignin decomposition during pyrolysis and ultimately increasing the yield. However, based on thermogravimetric curve analyses (Figure 1B), excessive preoxidation at elevated temperatures may result in oxidative losses and consequently lead to reduced yields.

Immediately following this, the synthesis condition was thoroughly investigated to achieve high-performance hard carbon. As shown in our results (see Text S2 and Figures S3–S7 for more information), a high temperature of 1400°C is beneficial for the preparation of hard carbon. A gas-phase removal-assisted aqueous washing strategy was devised to eliminate the sodium components from hard carbon prepared from industrial lignin, based on the low boiling point (882.8°C) of the sodium and the good aqueous solubility of sodium salts. All the process flows are shown in Figure 2A (samples denote 700BW, 700AW, L-1400BW, L-1400AW, 1000BW, 1000AW, H-1400BW, and H-1400AW; BW = before washing, AW = after washing; L = low temperature, H = high temperature, and the numbers represent the temperature). The surface compositions and chemical states of elements in a series of lignin-derived carbon materials were investigated using X-ray photoelectron spectroscopy (XPS) (Figure 2B, detailed analysis in Text S3). The XPS trend indicates that a higher temperature front-end heat treatment can expedite the migration of sodium to the material's surface (Figure 2C), thereby facilitating its removal through the subsequent aqueous washing.[24] By implementing this strategy, we successfully achieved H-1400BW samples with significantly reduced surface sodium content, while the H-1400AW samples showed a complete absence of sodium components on their surfaces.

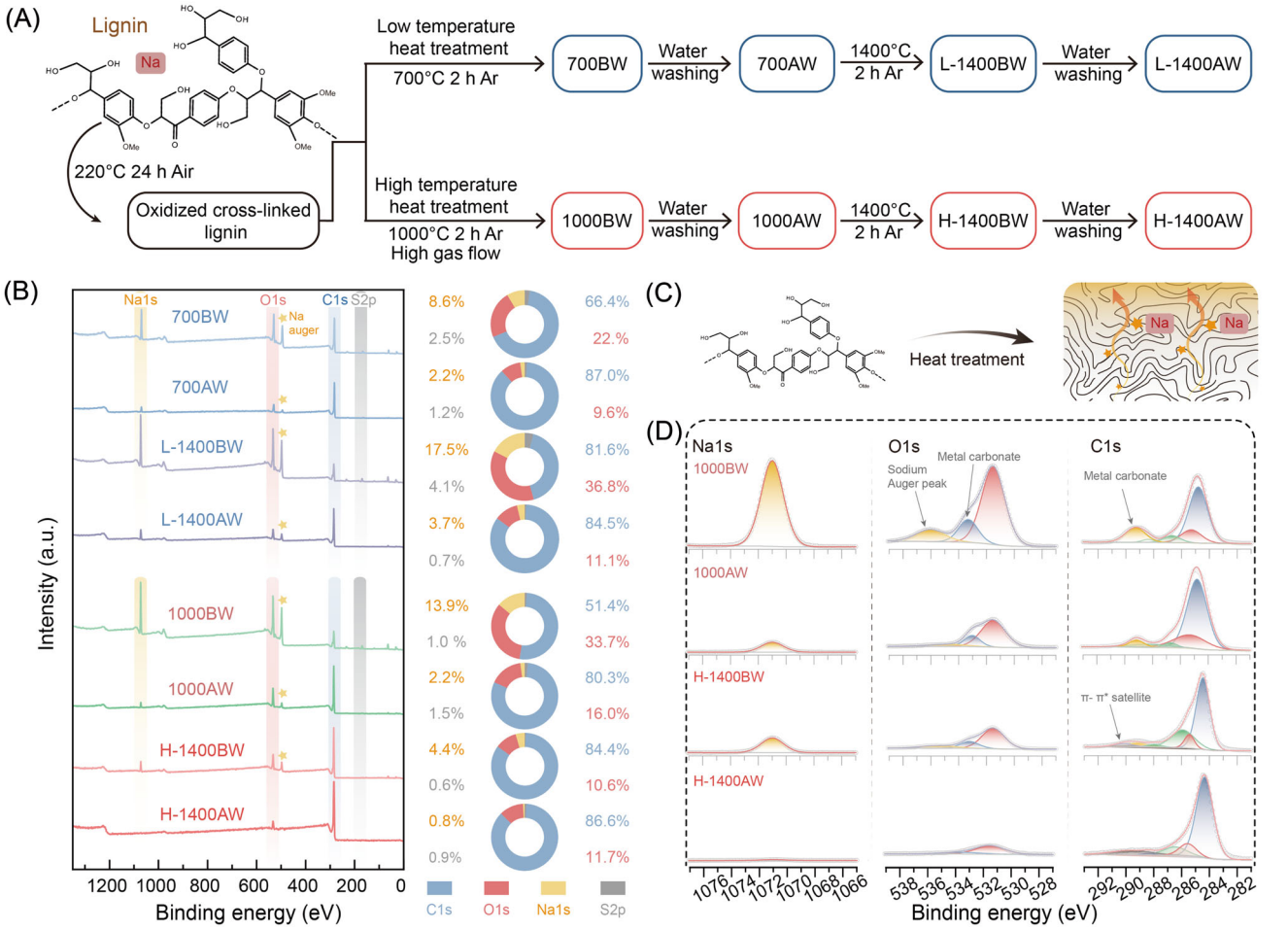

FIGURE 2 (A) Preparation of hard carbon for SIBs using lignin by both high- and low-temperature pyrolysis routes at the front end, respectively. (B) XPS survey spectra of different samples. The right side of the graph shows the relative element contents calculated using XPS results. (C) Schematic diagram of sodium migration during lignin pyrolysis. (D) High-resolution Na 1s, O 1s, and C 1s XPS spectra of different samples.

To elucidate the specific form of sodium components on the surface of hard carbon and evaluate its suitability within the electrode material, the high-resolution Na 1s, O 1s, and C 1s spectra of lignin-derived materials are also examined (Figures 2D and S8). The binding energy at 1071 eV can be assigned to sodium compounds,[25] with their contents changing throughout the process steps, and the presence of Na_2CO_3 in C 1s and O 1s is also consistent with the changes in the sodium content. The X-ray diffraction patterns of the 1000BW and H-1400BW samples show that the gas-phase removal-assisted aqueous washing process effectively removes most of the sodium components and also confirm that the sodium components that migrate to the carbon surface are in the form of Na_2CO_3 (Figure S9). It has been demonstrated that Na_2CO_3 is an important component of SEI membranes for SIBs,[26] so the role of these sodium components remaining on the carbon surface in the electrochemical performance is highly anticipated. Furthermore, we also investigated the morphological characteristics of the prepared samples and further established the structural features of their hard carbon (Figures S10–S12). To sum up the observations from experimental characterizations, we successfully synthesized hard carbon samples from industrial lignin using a gas-phase removal-assisted aqueous washing process.

2.2 | Electrochemical testing and electrochemical kinetic analysis

In an attempt to evaluate the effect of the residual sodium components on electrochemistry and electrode kinetics, the half-cell configuration was used to investigate the capacity of hard carbons in sodium ion storage. The cycling performance and galvanostatic charge–discharge curves of the H-1400BW and H-1400AW samples are illustrated in Figure 3A,B, demonstrating the exceptional

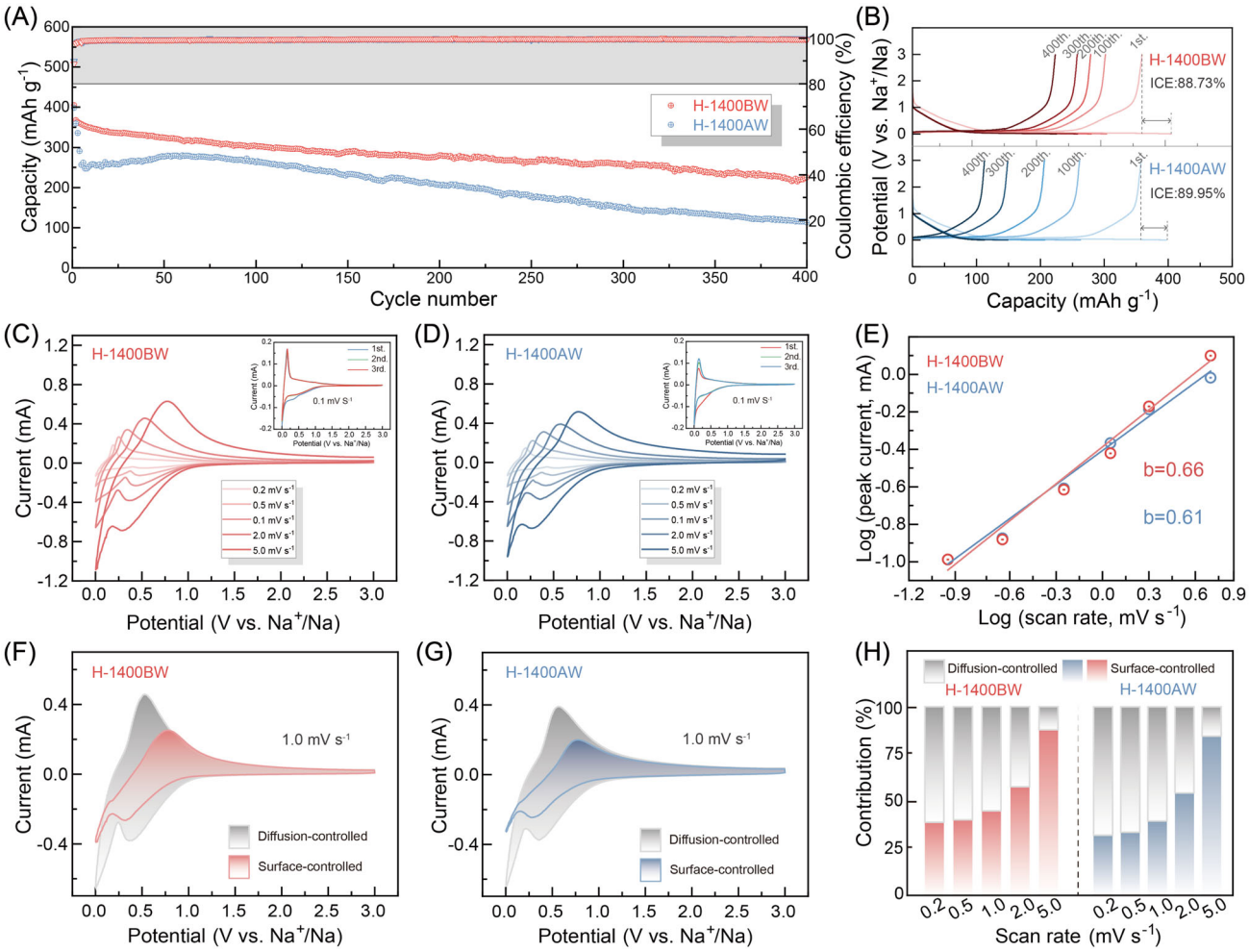

FIGURE 3 (A) Cycling performance of hard carbon cells using different electrodes cycled at 0.1 C (1.0 C = 300 mA g^{-1}). (B) Galvanostatic charge–discharge curves of different cycles of the H-1400BW electrode and the H-1400AW electrode. CV profiles (the inset shows the first three cycles' curves) with different sweep speeds for (C) the H-1400BW electrode and (D) the H-1400AW electrode. (E) Linear relationship between log(v) and log(i) of the H-1400BW electrode and the H-1400AW electrode. CV curves of (F) H-1400BW and (G) H-1400AW at 1.0 mV s^{-1} with surface control and diffusion control currents separated at each potential. (H) Capacitive contribution ratio of the H-1400BW electrode and the H-1400AW electrode in SIBs at scan rates ranging from 0.2 to 5.0 mV s^{-1}.

sodium storage capabilities of lignin-derived hard carbon (H-1400BW: 359 mAh g^{-1}), which is one of the highest values based on previous publications (Figure S13). The long low-potential plateau implies that most of the sodium ions are stored in the form of filled holes, which corresponds to the shoulder peaks observed by our small-angle X-ray scattering (Figure S12). It is noteworthy that H-1400BW, which has a small number of sodium residues on the hard carbon surface, demonstrates improved cycling stability and capacity retention. Further charge–discharge curve analyses showed that both the sharp capacity drop at the beginning of the cycle and the capacity decay at the end of the cycle mainly occurred in the plateau region at low potential (Figures S14 and S15), which is closely linked to the interfacial nature of the hard carbon surface. Therefore, the residual sodium components may play a key role in stabilizing the interphase and thus enhancing the electrochemical performance.

To clarify the effect of the residual sodium components on the electrode kinetics, first, cyclic voltammetry (CV) curves (scan rates [v] of 0.1−5.0 mV s^{-1}) of the cells were constructed (Figure 3C,D). Both samples present similar electrochemical behaviors at various v, but H-1400BW has a relatively larger peak current (i), emphasizing its superior electrochemical kinetics. Next, the relationship between v and i of CV is analyzed using the equation, $i = av^b$, to examine sodium-storage behaviors of both anodes, where a and b are constants. Figure 3E shows an excellent linear relationship between log(v) and log(i), yielding the calculated b values of 0.66 and 0.61 for H-1400BW and H-1400AW, respectively, and this suggests a combination of pseudocapacitive- and

diffusive-controlled sodium-storage processes in H-1400BW and H-1400AW. The contribution of the two controls discussed above can be further calculated by the equation, $i = k_1 v + k_2 v^{\frac{1}{2}}$ ($k_1 v$ and $k_2 v^{\frac{1}{2}}$ correspond to the pseudocapacitance and diffusion contributions, respectively, where k_1 and k_2 are constants), and the results are shown in Figure 3F–H. At a v of $1.0\,\mathrm{mV\,s^{-1}}$, the pseudocapacitance of H-1400BW is calculated to be 44.8%, which is higher than that of H-1400AW (39.4%), and as v increases, the pseudocapacitive contribution of H-1400BW becomes more apparent. The high pseudocapacitance ratio indicates that the material favors surface redox reactions or that the electrode provides a favorable ion transport and adsorption path.[27,28] The increased intercalation pseudocapacitance triggered by H-1400BW indicates faster diffusion and electron transport of sodium ions throughout the cell.[29]

Considering that the distinguishing factor between the two electrodes lies in the presence of residual sodium components on the surface of hard carbon, our investigation next focuses on the electrochemical kinetics of interphases, as it plays a crucial role in ensuring consistent cycling performance of the cell.[30,31] Remarkably, the structural characteristics of the interphases are well reflected by the alternating current (AC) impedance.[32] Nyquist plots of in situ electrochemical impedance spectroscopy (EIS) of H-1400BW and H-1400AW during discharge–charge processes are shown in Figure 4A,B. The charge-transfer resistance (R_{ct}) of both in discharging is significantly higher than that in charging, which indicates that the resistance of the hard carbon material is significantly larger during sodium insertion than sodium desertion, due to the formation of SEI. It is worth noting that, as shown in Figure 4C, H-1400BW shows a rapid reduction in R_{ct} at the beginning of the discharge, with R_{ct} reducing to a smaller value than H-1400AW during the first discharge. Moreover, the reactive sodium ion migration using the galvanostatic intermittent titration technique (GITT) indicates that H-1400BW shows a relatively higher diffusion coefficient, indicative of the fast ion transport (Figure 4D,E). Taken together, the robust interphase of H-1400BW is the key to improved cycling performance.

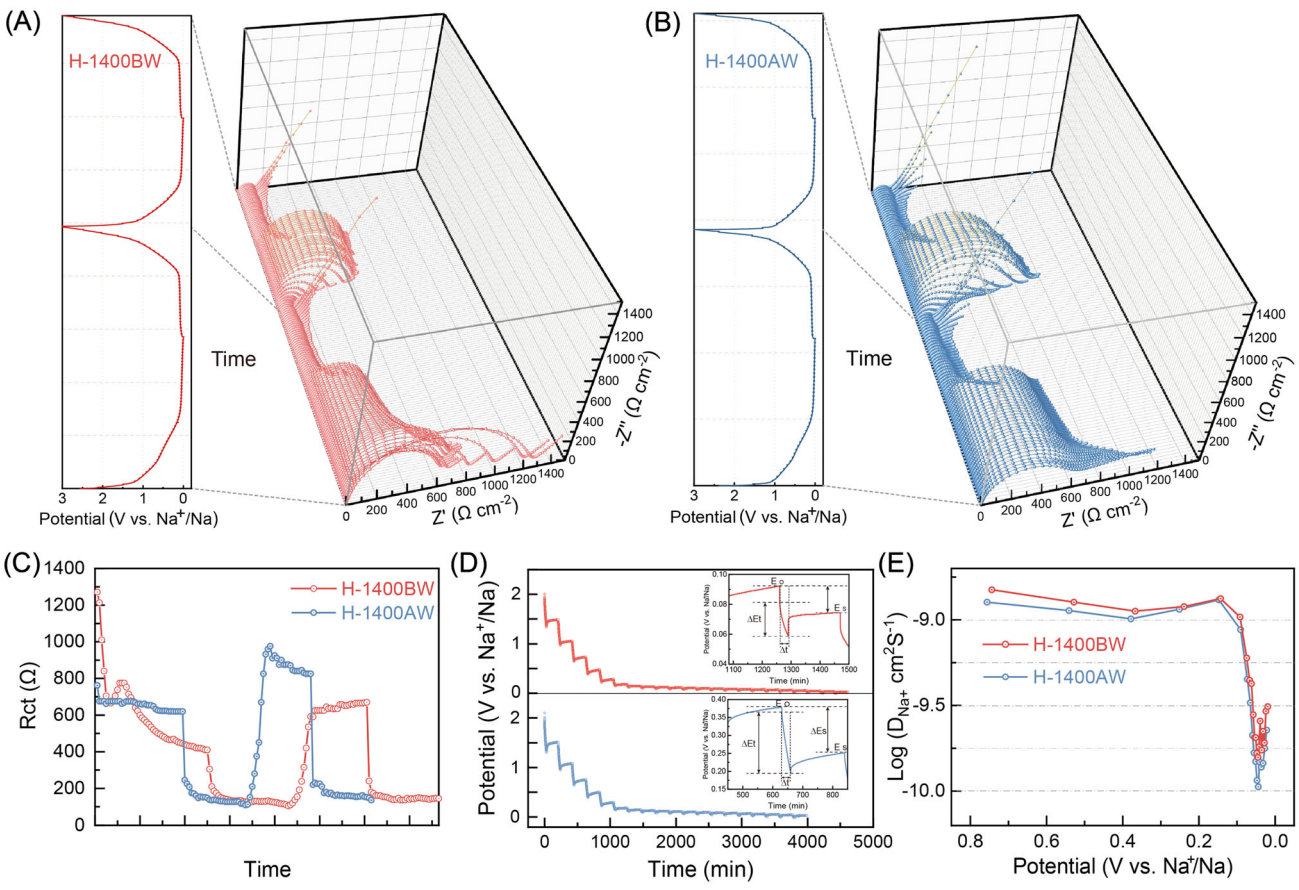

FIGURE 4 In situ EIS of (A) the H-1400BW electrode and (B) the H-1400AW electrode in the first two galvanostatic discharge–charge processes. (C) Corresponding R_{ct} of the H-1400BW electrode and the H-1400AW electrode (D) GITT potential profiles of H-1400BW and H-1400AW. (E) Calculated Na^+ diffusion coefficients of the H-1400BW electrode and the H-1400AW electrode.

2.3 | Fundamental insights into interfacial phenomena

After confirming that excellent electrochemical performance depends on robust interphases, the remaining issue is the impact of the residual sodium components on the physical and chemical properties of SEI. First, we investigated the composition and content of SEI on hard carbon surfaces. Time-of-flight secondary ion mass spectrometry (TOF-SIMS) for the H-1400BW electrode and the H-1400AW electrode after the first cycle was performed in the range of positive polarity. Analysis of a large number of SEI fragments from the H-1400BW electrode and the H-1400AW electrode indicates considerable similarity in their SEI composition (Figure 5A), with SEI fragments mainly assigned to sodium-containing inorganic contents (62 [Na_2O^+], 63 [Na_2OH^+], 65 [Na_2F^+], 85 [Na_3O^+], 107 [$Na_3F_2^+$], and 129 [$Na_3CO_3^+$]).[26] Notably, there were considerable differences in these inorganic contents. The changes in SEI can be attributed to the presence of residual sodium components on the surface of the hard carbon. Otherwise, the morphology of SEI on both samples was found to be different in terms of structure and thickness when we compared their

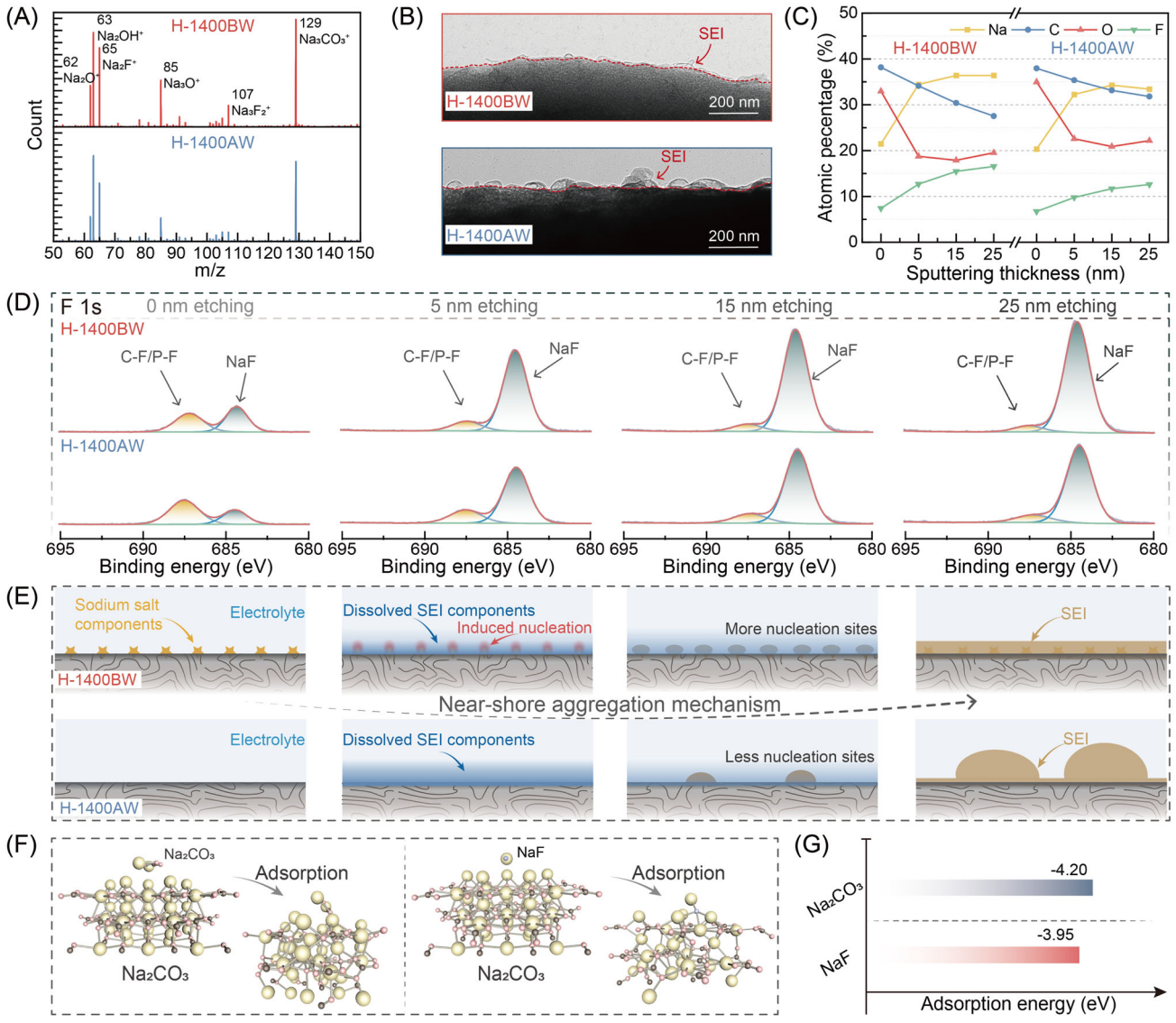

FIGURE 5 (A) TOF-SIMS spectra for the H-1400BW electrode and the H-1400AW electrode after the first cycle. (B) High-resolution transmission electron microscopy image of the H-1400BW electrode and the H-1400AW electrode after the first cycle. (C) Variation of the atomic content of the H-1400BW electrode and the H-1400AW electrode after the first cycle measured by XPS at different sputtering thicknesses. (D) F 1s XPS spectra of the H-1400BW electrode and the H-1400AW electrode. (E) Schematic pictures of SEI formation processes based on the near-shore aggregation mechanism. (F) Simulated interaction configurations and (G) calculated adsorption energy between the nucleation center (Na_2CO_3) and the main SEI components of Na_2CO_3 and NaF.

transmission electron microscopy images (Figure 5B). The SEI of H-1400BW is relatively thin and dense, with a uniform film layer, while that of H-1400AW has a hemispherical pile-up on the material's surface.

Besides content and morphology, the spatial distribution of SEI components also has a profound impact on the cycling stability of electrodes. To understand the effect of residual sodium components, Ar^+ sputtering was used to probe different depths of the SEI layer. With an increase in the etching depth, the inner SEI of H-1400BW contains more sodium and fluorine components with fewer carbon and oxygen contents than that of H-1400AW (Figure 5C). In particular, the F 1s XPS spectra show that the NaF content in the SEI of H-1400BW increases significantly with increasing etching depth (Figure 5D).[33,34] Previous studies have demonstrated that inorganic NaF-rich SEI layers are more resistant to stress changes during cycling, thus resulting in better structural stability.[35] In addition, the high-resolution C 1s XPS spectra show relatively lower contents of alkyl carbonate and sodium carbonate and higher contents of organic carbon in the SEI of H-1400BW (Figure S16).[27,36] Based on this, it can be deduced that H-1400BW is enriched with inorganic NaF and organic components of SEI to ensure its long-cycle stability, with all of the performance–structure differences attributed to the reconstruction of the SEI due to the transition of sodium residues to integrate SEI compositions.

Considering the key role that residual sodium components play in hard carbon, we further investigated the underlying mechanism. For this, we analyzed typical patterns in the formation of SEI. Two typical growth mechanisms for SEI have been reported: the nanoscale SEI "surface growth" model, which combines classical molecular dynamics and Monte Carlo methods,[37] and the "near-shore aggregation" mechanism reported by Ushirogata et al.[38] For the mechanism of "near-shore aggregation," it is proposed that the SEI components formed at the electrode surface desorb into the near-shore region and aggregate, subsequently coalescing and contacting the electrode to complete SEI formation. Given the higher solubility of SEI in SIBs,[39,40] it can be inferred that the growth mechanism of SEI in SIBs is more inclined towards near-shore aggregation, as illustrated in Figure 5E. As a result of the residual sodium salt component on the hard carbon surface, we may infer that the interphase of H-1400BW is nucleation-based growth, resulting in a thin and dense SEI. The H-1400AW sample, on the other hand, lacks a nucleation center and the SEI growth is dominated by nuclei growth, which in turn leads to hemispherical large particles with uneven SEI components.

To further validate our proposed hypothesis, a density functional theory calculation is performed. We performed simulation of the interactions between residual salt components (e.g., Na_2CO_3) on the surface of the material and the main SEI components (e.g., Na_2CO_3 and NaF as detected by XPS) (Figure 5F). The calculated adsorption energies of Na_2CO_3 and NaF inorganics on the Na_2CO_3 slab show that the residual surface Na_2CO_3 has a high affinity for both Na_2CO_3 and NaF components (Figure 5G), indicating that the sodium salts remaining on the hard carbon surface interact strongly with the SEI membrane components dissolved in the electrolyte. This will promote SEI nucleation and uniform growth. The computational results adequately account for the experimental observations and clarify the real SEI growth behavior in our studied system.

3 | CONCLUSIONS

Lignin-derived hard carbon was synthesized using a gas-phase removal-assisted aqueous washing process. The as-synthesized hard carbon anode shows remarkable sodium storage performance on evaluation as an anode material for SIBs. One of the key findings to emerge from this study is that the residual sodium components on the hard carbon surface play an important role in SEI formation; specifically, they can modulate both the composition and morphology of the SEI, thereby yielding robust interphases. Theoretical calculations have verified our finding and confirmed that migration of sodium carbonate to the hard carbon surface helps to promote nucleation and homogeneous growth of SEI. These findings are crucial for comprehending the process of synthesizing high-performance hard carbon and elucidating the formation and regulation mechanisms of SEI in SIBs.

ACKNOWLEDGMENTS

The authors are grateful for the grants provided by the National Natural Science Foundation of China (Grant no. 52274309) and the Postgraduate Scientific Research Innovation Project of Hunan Province (Grant no. CX20220183). Simin Li thanks the National Natural Science Foundation of China (Grant no. 52204327).

CONFLICT OF INTEREST STATEMENT

The authors declare that there are no conflicts of interests.

ORCID

Zhian Zhang http://orcid.org/0000-0002-8691-6006

REFERENCES

1. Zhang B-W, Sheng T, Liu Y-D, et al. Atomic cobalt as an efficient electrocatalyst in sulfur cathodes for superior room-temperature sodium–sulfur batteries. *Nat Commun*. 2018;9(1):4028.
2. Zhong X, Duan J, Xiang Y, et al. Constructing rich interfacial structure by carbon dots to improve the sodium storage capacity of Sb/C composite. *Adv Funct Mater*. 2023;33(52):2306574.
3. Zhao C, Wang Q, Yao Z, et al. Rational design of layered oxide materials for sodium-ion batteries. *Science*. 2020;370(6517):708-711.
4. Vaalma C, Buchholz D, Weil M, Passerini S. A cost and resource analysis of sodium-ion batteries. *Nat Rev Mater*. 2018;3(4):18013.
5. Huang Y, Zhong X, Hu X, et al. Rationally designing closed pore structure by carbon dots to evoke sodium storage sites of hard carbon in low-potential region. *Adv Funct Mater*. 2023;34(4):2308392.
6. Asher RC, Wilson SA. Lamellar compound of sodium with graphite. *Nature*. 1958;181(4606):409-410.
7. Metrot A, Guerard D, Billaud D, Herold A. New results about the sodium-graphite system. *Synth Met*. 1980;1(4):363-369.
8. Akuzawa N, Yoshioka J, Ozaki C, Tokuda M, Ohkura K, Soneda Y. Preparation and characterization of sodium–graphite intercalation compounds. *Mol Cryst Liq Cryst*. 2002;388(1):1-7.
9. Stevens DA, Dahn JR. High capacity anode materials for rechargeable sodium-ion batteries. *J Electrochem Soc*. 2000;147(4):1271-1273.
10. Dou X, Hasa I, Saurel D, et al. Hard carbons for sodium-ion batteries: structure, analysis, sustainability, and electrochemistry. *Mater Today*. 2019;23:87-104.
11. Liu M, Wu F, Gong Y, et al. Interfacial-catalysis-enabled layered and inorganic-rich SEI on hard carbon anodes in ester electrolytes for sodium-ion batteries. *Adv Mater*. 2023;35(29):2300002.
12. Bommier C, Leonard D, Jian Z, Stickle WF, Greaney PA, Ji X. New paradigms on the nature of solid electrolyte interphase formation and capacity fading of hard carbon anodes in Na-ion batteries. *Adv Mater Interfaces*. 2016;3(19):1600449.
13. Muñoz-Márquez MÁ, Saurel D, Gómez-Cámer JL, Casas-Cabanas M, Castillo-Martínez E, Rojo T. Na-ion batteries for large scale applications: a review on anode materials and solid electrolyte interphase formation. *Adv Energy Mater*. 2017;7(20):1700463.
14. Chu Y, Zhang J, Zhang Y, et al. Reconfiguring hard carbons with emerging sodium-ion batteries: a perspective. *Adv Mater*. 2023;35(31):2212186.
15. Watkins D, Nuruddin M, Hosur M, Tcherbi-Narteh A, Jeelani S. Extraction and characterization of lignin from different biomass resources. *J Mater Res Technol*. 2015;4(1):26-32.
16. Klett AS, Chappell PV, Thies MC. Recovering ultraclean lignins of controlled molecular weight from Kraft black-liquor lignins. *Chem Commun*. 2015;51(64):12855-12858.
17. Li Y, Hu Y-S, Li H, Chen L, Huang X. A superior low-cost amorphous carbon anode made from pitch and lignin for sodium-ion batteries. *J Mater Chem A*. 2016;4(1):96-104.
18. Wang Y, Xiao N, Wang Z, et al. Ultrastable and high-capacity carbon nanofiber anodes derived from pitch/polyacrylonitrile for flexible sodium-ion batteries. *Carbon*. 2018;135:187-194.
19. Xu W, Dang R, Zhou L, et al. Conversion of surface residual alkali to solid electrolyte to enable Na-ion full cells with robust interfaces. *Adv Mater*. 2023;35(42):2301314.
20. Crestini C, Lange H, Sette M, Argyropoulos DS. On the structure of softwood kraft lignin. *Green Chem*. 2017;19(17):4104-4121.
21. Lu Y, Zhao C, Qi X, et al. Pre-oxidation-tuned microstructures of carbon anodes derived from pitch for enhancing Na storage performance. *Adv Energy Mater*. 2018;8(27):1800108.
22. Cao J, Yu Y, Wu H. Primary release and transformation of inorganic and organic sodium during fast pyrolysis of sodium-loaded lignin. *Proc Combust Inst*. 2023;39(3):3439-3446.
23. Zhang X, Yan Q, Leng W, et al. Carbon nanostructure of Kraft lignin thermally treated at 500 to 1000°C. *Materials*. 2017;10(8):975.
24. Leijenhorst EJ, Wolters W, van de Beld L, Prins W. Inorganic element transfer from biomass to fast pyrolysis oil: review and experiments. *Fuel Process Technol*. 2016;149:96-111.
25. Yin X, Lu Z, Wang J, et al. Enabling fast Na^+ transfer kinetics in the whole-voltage-region of hard-carbon anodes for ultrahigh-rate sodium storage. *Adv Mater*. 2022;34(13):2109282.
26. Komaba S, Murata W, Ishikawa T, et al. Electrochemical Na insertion and solid electrolyte interphase for hard-carbon electrodes and application to Na-ion batteries. *Adv Funct Mater*. 2011;21(20):3859-3867.
27. Zhen X, Jing W, Zhenyu G, et al. The role of hydrothermal carbonization in sustainable sodium-ion battery anodes. *Adv Energy Mater*. 2022;12(18):2200208.
28. Jing W, Zhen X, Jean-Charles E, Maria-Magdalena T, Stephen JE. Ice-templated, sustainable carbon aerogels with hierarchically tailored channels for sodium- and potassium-ion batteries. *Adv Funct Mater*. 2022;32(16):2110862.
29. Liu Y, Wan Y, Zhang JY, et al. Surface stretching enables highly disordered graphitic domains for ultrahigh rate sodium storage. *Small*. 2023;19(28):2301203.
30. Jin Y, Le PML, Gao P, et al. Low-solvation electrolytes for high-voltage sodium-ion batteries. *Nat Energy*. 2022;7(8):718-725.
31. Barsoukov E. Comparison of kinetic properties of $LiCoO_2$ and $LiTi_{0.05}Mg_{0.05}Ni_{0.7}Co_{0.2}O_2$ by impedance spectroscopy. *Solid State Ion*. 2003;161(1-2):19-29.
32. Rangom Y, Gaddam RR, Duignan TT, Zhao XS. Improvement of hard carbon electrode performance by manipulating SEI formation at high charging rates. *ACS Appl Mater Interfaces*. 2019;11(38):34796-34804.
33. Fondard J, Irisarri E, Courrèges C, Palacin MR, Ponrouch A, Dedryvère R. SEI composition on hard carbon in Na-ion batteries after long cycling: influence of salts ($NaPF_6$, NaTFSI) and additives (FEC, DMCF). *J Electrochem Soc*. 2020;167(7):070526.
34. Fang H, Gao S, Ren M, et al. Dual-function presodiation with sodium diphenyl ketone towards ultra-stable hard carbon anodes for sodium-ion batteries. *Angew Chem Int Ed*. 2023;62(2):202214717.
35. Wang H, Zhu C, Liu J, et al. Formation of NaF-rich solid electrolyte interphase on Na anode through additive-induced anion-enriched structure of Na^+ solvation. *Angew Chem*. 2022;134(38):202208506.
36. Li L, Cheng D, Zou G, Hou H, Ji X, Yang L. Carbon anode from carbon dots-regulated polypyrrole for enhanced potassium storage. *J Alloys Compd*. 2023;958:170481.
37. Takenaka N, Suzuki Y, Sakai H, Nagaoka M. On electrolyte-dependent formation of solid electrolyte interphase film in

lithium-ion batteries: strong sensitivity to small structural difference of electrolyte molecules. *J Phys Chem C*. 2014;118(20):10874-10882.
38. Ushirogata K, Sodeyama K, Futera Z, Tateyama Y, Okuno Y. Near-shore aggregation mechanism of electrolyte decomposition products to explain solid electrolyte interphase formation. *J Electrochem Soc*. 2015;162(14):A2670-A2678.
39. Mogensen R, Brandell D, Younesi R. Solubility of the solid electrolyte interphase (SEI) in sodium ion batteries. *ACS Energy Lett*. 2016;1(6):1173-1178.
40. Le Anh M, Andrew JN, Leif N, Reza Y. Strategies for mitigating dissolution of solid electrolyte interphases in sodium-ion batteries. *Angew Chem Int Ed*. 2020;60(9):4855-4863.

SUPPORTING INFORMATION

Additional supporting information can be found online in the Supporting Information section at the end of this article.

How to cite this article: Zheng J, Wu Y, Guan C, et al. Lignin-derived hard carbon anode with a robust solid electrolyte interphase for boosted sodium storage performance. *Carbon Energy*. 2024;6:e538. doi:10.1002/cey2.538